



Effect of Temperature Gradient in Ash on High-Temperature Corrosion of Super-Heater Material in a Waste Power Generation Boiler

T. Furugaki¹ · H. Takahashi¹ · S. Hayashi²

Received: 10 June 2022 / Revised: 19 September 2022 / Accepted: 1 October 2022 /
Published online: 26 October 2022

© The Author(s), under exclusive licence to Springer Science+Business Media, LLC, part of Springer Nature 2022

Abstract

The effect of a temperature gradient associated with ash deposition on the high-temperature corrosion behavior of heat-resistant steels used for super-heater tubes in a waste-to-energy (WTE) boiler plant was investigated by conducting ash embedded corrosion tests using combustion ash from the actual boiler. The ash-embedded corrosion test was carried out under two conditions: (1) an isothermal corrosion test at 460 °C, and (2) a temperature-gradient corrosion test with a specimen temperature of 460 °C; and an atmospheric temperature of 685 °C in air. The corrosion mass loss was found to be much greater under higher atmospheric temperatures where the same specimen temperature was maintained than under the same atmospheric temperatures where the specimen temperature was kept at a constant 460 °C. Cross-sectional observations of the ash after the temperature gradient corrosion test revealed that the alkali salt mixture was melted in the region above the melting point of the ash, however, no penetration of the melt reaching to the specimen surface was confirmed, suggesting that the corrosion was produced by a gas–solid reaction. Thus, the faster corrosion kinetics of the heat-resistant steels under an ash deposit with a temperature gradient can be attributed to breakdown of an initially formed protective Cr-rich oxide scale by a reaction with a vapor of alkali salts to form less protective alkaline chromates. The difference in the potentials of the alkali salt across the ash deposit due to the temperature gradient could be the driving force that increases the flux of the alkali salts toward the specimen surface, which accelerates the formation of chromates and the rate of breakdown of the protective Cr-rich oxide scale.

Keywords High-temperature corrosion · Temperature gradient · Ash · Alkali salt vapor · Heat-resistant steel · Cr-rich oxide scale

✉ T. Furugaki
furugaki@takuma.co.jp

Extended author information available on the last page of the article

Introduction

Waste power generation and biomass power generation play an important role in energy supply. Due to a reduction in the power generated by fossil fuel combustion, the importance of WTE plants is now increasing. Higher steam temperature is one of the crucial requirements to increase the efficiency of WTE plants. However, the steam temperature in current WTE plants is much lower than that in fossil fuel power plants because of the high-temperature corrosion of components used in the boiler. Super-heater tubes used in waste incineration plants are exposed to extremely corrosive environments, which contain corrosive gas. Combustion ash, which contains alkaline salts and heavy metal salts, also accelerates corrosion through deposition on the surface of super-heater tubes during service. In such a severely corrosive environment, various coatings are used to protect the super-heater tubes of WTE plants, which are typically made from Type 310 heat-resistant steel [1–4].

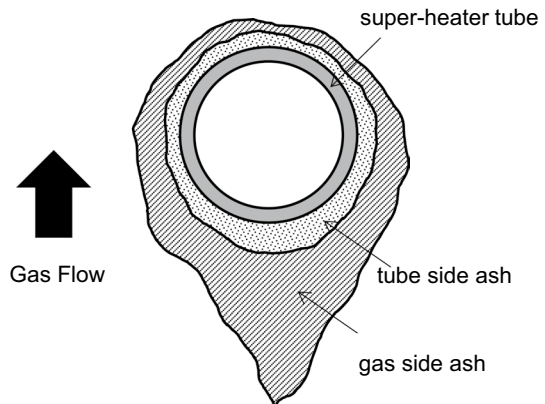
It is well known that enhanced oxidation degradation, so called active oxidation, occurs on oxidation resistant alloys in chlorine-containing atmospheres due to simultaneous oxidation and chlorination reactions within the oxide scale when chlorine penetrates the oxide scale to the metal/oxide scale interface. Under “active oxidation,” metal chlorides generated by chlorination of a metal substrate or oxides within the oxide scale where the oxygen potential is sufficiently low are oxidized to form a very porous, sponge-like oxide scale that is less protective. Once active oxidation takes place, rapid corrosion continues to progress even if chlorine is not continuously supplied from the gas atmosphere. This situation accelerates the oxidation/corrosion of alloys [5–7].

An external chromium oxide (Cr_2O_3) has the ability to protect steel against chlorination atmospheres to some extent. However, over the long term, it loses its protective function. While the routes by which chlorine penetrates the metal/oxide scale interface still require elucidation, one route has been reported to be via cracks and pores in the Cr oxide scale [4]. Moreover, it has also been shown that in a harsh environment characterized by high gas and steam temperatures, the protective Cr oxide scale is destroyed by corrosive factors, such as alkali chlorides. Alkali chlorides have also been reported to form alkali chromates by reacting with Cr_2O_3 scale, which also decreases the protective ability of the Cr-rich oxide scale. [8–14]

Under the operational conditions of the boiler, heat-resistant steels used for super-heater tubes are exposed to an extremely corrosive environment containing several corrosive gas species such as HCl, SO_2 , O_2 , H_2O , and CO_2 . The combustion ash, which is mainly composed of various salts, deposited on the surface of tubes is also known to accelerate corrosion [15]. Many studies have evaluated the corrosion behavior of heat-resistant steels and alloys in various ash embedding conditions, however, “most these studies were conducted as a crucible test,” in which the samples were embedded in the ash or various salt mixtures in a crucible and exposed isothermally to different temperatures. In an actual boiler, because of differences in the temperatures in the atmosphere and steam, a large temperature

Table 1 Chemical composition of super-heater tube materials (nominal in mass%)

	Si	Mo	N	Cr	Ni	Fe
SUS310S	≤1.50	—	—	24.0~26.0	19.0~22.0	Bal
Q562	2.50~3.50	1.00~2.00	0.042	24.0~26.0	22.0~25.0	Bal

Fig. 1 Schematic cross section of combustion ash deposited on super-heater tube

gradient exists across the ash deposited on a super-heater tube. Reports show that this temperature gradient accelerates the corrosion [16]; however, the role of the temperature gradient on the corrosion behavior of heat-resistant steels and alloys is yet to be fully clarified. In this study, corrosion tests were conducted using combustion ash collected from an actual super-heater tube, and the effect of the temperature gradient in the ash on the high-temperature corrosion behavior of steels was investigated.

Experimental Procedures

Sample Preparation

Specimens for corrosion tests were cut from commercial SUS310S and Q562 steel tubes into $10 \times 10 \times 1$ mm coupons. All specimen surfaces were polished with a SiC paper up to 4000 grits and finished with a $3 \mu\text{m}$ diamond paste. Before corrosion tests, the specimens were ultrasonically degreased and cleaned in acetone for 10 min. Nominal compositions of the steels used are shown in Table 1.

Combustion Ash

In this study, combustion ash deposited on the surface of super-heater tubes in an actual waste incineration boiler was used in the corrosion tests. Figure 1 shows a

Table 2 Ash composition by XRF (in mass%)

	Ca	O	Cl	K	Si	S	Na	Al	Ti	Fe	Mg	Zn	C	Pb	Ca:Na:K
tube side	20.7	19.0	31.3	9.5	1.8	2.9	9.6	1.5	0.7	0.5	0.7	0.6	0.0	0.05	2:1:1
gas side	28.6	34.3	11.4	3.0	3.8	3.6	2.6	3.6	1.6	1.2	1.5	0.7	2.3	0.03	10:1:1

schematic cross section of the combustion ash deposited on a super-heater tube, and Table 2 shows the composition of the combustion ash sampled at different depths of the deposit by XRF (X-ray fluorescence). The alkali chloride content in the tube side ash was much higher at 31.3 mass% in comparison with the gas side ash at 11.4 mass%. Conversely, the oxide content in the gas side ash was higher than that in the tube side ash. Of these ash samples, the tube side ash, which was rich in alkali salts and highly corrosive, was used for the corrosion tests. The melting point of the tube side ash was confirmed by TG–DTA to be 519 °C.

Corrosion Tests

Corrosion tests were performed in a furnace in air for 100 h. Tests were conducted either isothermally, where the atmosphere and specimens were set to the same temperature, or non-isothermally, i.e., the temperature of the atmosphere was set higher than that of the specimens. The isothermal corrosion tests were

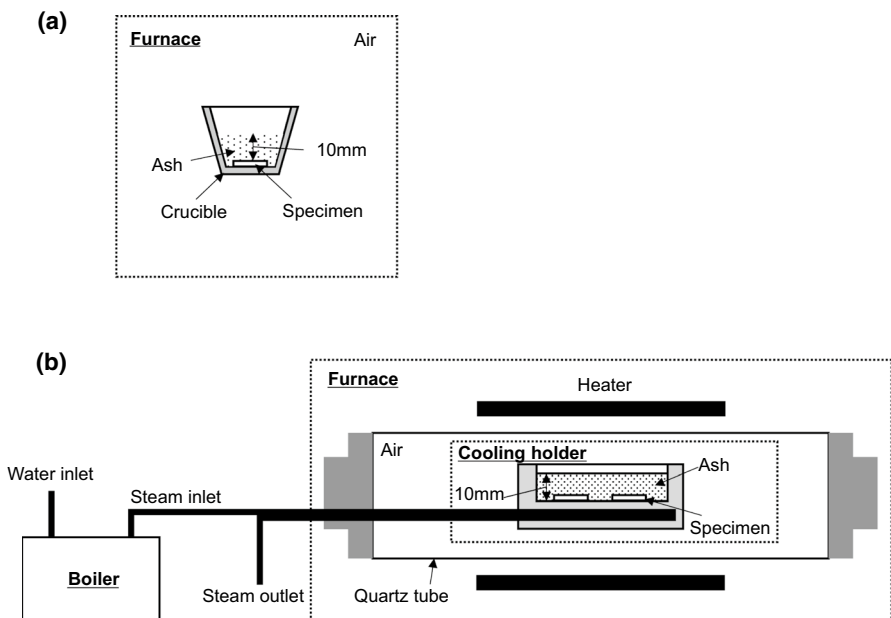


Fig. 2 Schematic of corrosion equipment: **a** isothermal corrosion test, **b** temperature gradient corrosion test

performed in a box furnace at 460 °C, as illustrated in Fig. 2(a). The specimens were embedded in the ash at a depth of 10 mm from the ash surface in an Al₂O₃ crucible. The non-isothermal corrosion tests were performed in an open horizontal tube furnace, as illustrated in Fig. 2(b). The specimens were embedded in the ash at a depth of 10 mm from the ash surface in the specimen holder and cooled by feeding steam into the specimen holder. During corrosion tests, the temperature of the atmosphere was set to 685 °C and that of the specimens was set to 460 °C. The temperature was monitored by thermocouples inserted in the reaction tube and the specimen holder.

At least two specimens of each type of steel underwent corrosion in each corrosion test. After the corrosion test, corrosion products formed on the one of the two specimens were removed by chemical treatment according to ISO 17248:2015E (see Table 3). The mass change of each specimen was evaluated by measuring the mass of specimens before corrosion and after the removal of oxide scale/corrosion products by chemical treatment. The other specimen was mounted in epoxy resin, then cut and polished using oil in order to prevent dissolution of reaction products in water. The cross section of the specimens was examined by scanning electron microscopy (SEM, JEOL JSM-IT200) with an accelerating voltage of 15 kV and electron probe micro-analyzer (EPMA, JEOL JXA-8530F) with an accelerating voltage of 15 kV to determine the microstructure and elemental distribution of the corrosion products. The specimens were also analyzed using X-ray diffraction (XRD; Rigaku SmartLab) to confirm the structural phases of the corrosion products. The XRD patterns were measured in Bragg–Brentano geometry using Cu- κ 1 radiation ($\lambda = 1.5405$ nm) in the range of 20° – 90° with a step size of 0.01 and 4 s per step. The analysis of XRD profiles was performed using QualX2 software with the POW_COD database for phase identification. In order to confirm the distribution of alkaline chlorides in the ash after the temperature gradient corrosion test, ash cross sections, which were non-heated or heated at 685 °C in a crucible with a lid for 2 h, and after a temperature gradient corrosion test for 100 h, were analyzed by SEM and energy dispersive spectroscopy (EDS). The temperature distribution in the ash was also measured using K-type thermocouples inserted in the ash at different depths (1, 3 and 7 mm) from the specimen surface.

Table 3 Chemical treatment procedure based on ISO 17428:2015(E)

	Chemical agents	Time (min)	Temperature
Step 1	90 g of sodium hydroxide (NaOH) 15 g of potassium permanganate (KMnO ₄) distilled water to make 500 ml	30	Boiling
Step 2	50 g ammonium citrate ((NH ₄) ₂ C ₂ H ₆ O ₇) distilled water to make 500 ml	30	Boiling

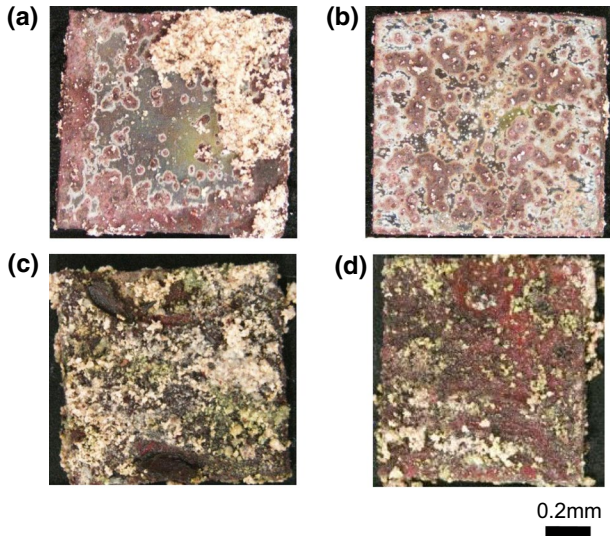


Fig. 3 Surface observations of specimen after corrosion for 100 h: **a** SUS310S after isothermal corrosion test, **b** QSX5 after isothermal corrosion test, **c** SUS310S after temperature gradient corrosion test, **d** QSX5 after temperature gradient corrosion test

Results

Surface Morphology of Specimens After Corrosion

Figure 3 shows the surface appearance of the specimens after undergoing corrosion for 100 h. After the isothermal corrosion test, localized areas of the specimen surface changed to a bright brown color, and the metallic regions with interference color remained in other areas. In addition, the bright-brown corroded areas appear to extend around those places where ash had accumulated. On the other hand, after the temperature gradient corrosion test, the corroded areas extended over the entire surface of the specimens with the corrosion products appearing as a dark brown color. Yellow and green colored reaction products can also be locally observed on the dark brown colored corrosion products combined with the white ash. These corrosion products are presumed to be Fe-rich oxides and Ca chromate, as described below.

Corrosion Mass Change

Figure 4 shows the mass loss of specimens after undergoing corrosion for 100 h. The corrosion mass loss of both steels was small in the isothermal corrosion test, but the mass loss of SUS310S tended to be greater than that of QSX5. However, in the temperature gradient corrosion test, it is obvious that the corrosion mass loss of SUS310S was much greater than that of QSX5, and the corrosion

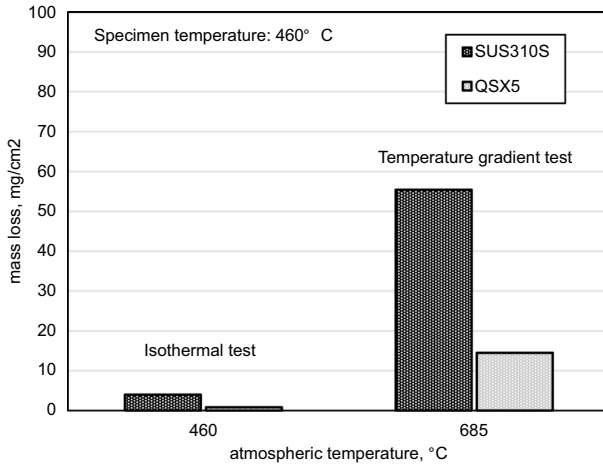


Fig. 4 Mass loss after corrosion for 100 h

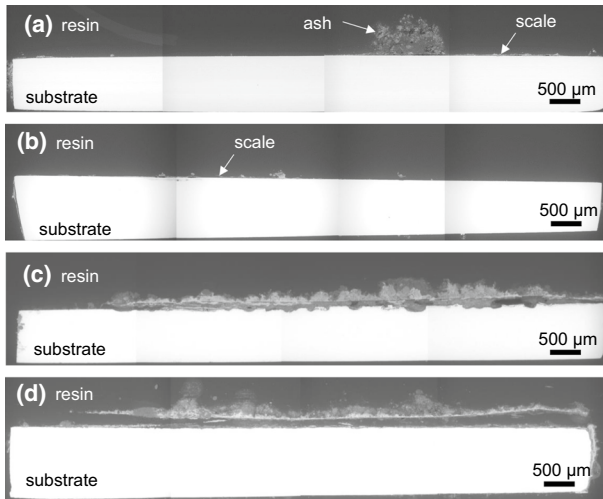


Fig. 5 Cross sections after corrosion for 100 h: **a** SUS310S after isothermal corrosion test, **b** QSX5 after isothermal corrosion test, **c** SUS310S after temperature gradient corrosion test, **d** QSX5 after temperature gradient corrosion test

mass loss of both steels was more than 10 times greater than that which occurred during the isothermal corrosion test. This finding indicates that the temperature gradient in the ash accelerates the corrosion rate even though the specimen temperature is the same.

Cross-Sectional Observation and Analysis of Specimens After Corrosion

Figure 5 shows the cross sections of the specimens after corrosion for 100 h. A thin oxide scale formed on part of the specimen surface, but no penetration of corrosion products into the specimen can be observed following the isothermal corrosion test as shown in Figs. 5(a), (b). However, almost the entire surface of both specimens became covered by a thick oxide scale following the temperature gradient corrosion test. Significant inward attack by can be observed in SUS310S and the surface of the specimen became very rough due to local penetration of corrosion products, as shown in Fig. 5(c). However, such penetration of corrosion products was not clearly evident on the QSX5 specimen as shown in Fig. 5(d). This finding suggests that QSX5 has higher resistance to corrosion than SUS310S under the corrosion conditions present in this test.

Figure 6 shows enlarged cross sections of the specimen following the temperature gradient corrosion test for 100 h. The scale structure was similar for both steels, and the scale formed on the steels can be divided into two parts. The outer part of the oxide scale is very porous, and the ash has been incorporated into the oxide scale. The inner part of the oxide scale has a layer-by-layer structure and appears to penetrate into the alloy substrate.

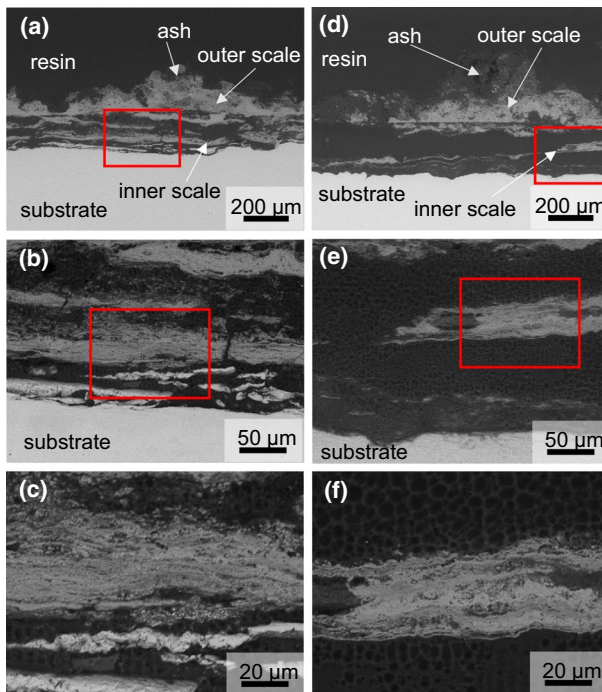


Fig. 6 Cross sections after temperature gradient corrosion test for 100 h: **a, b** and **c** SUS310S, **d, e** and **f** QSX5

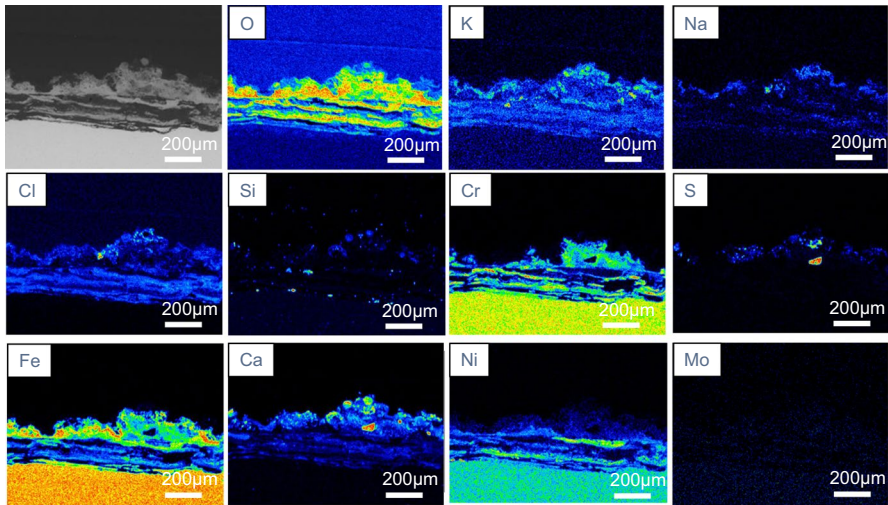


Fig. 7 Elemental distribution maps of the cross section of SUS310S after temperature gradient corrosion test

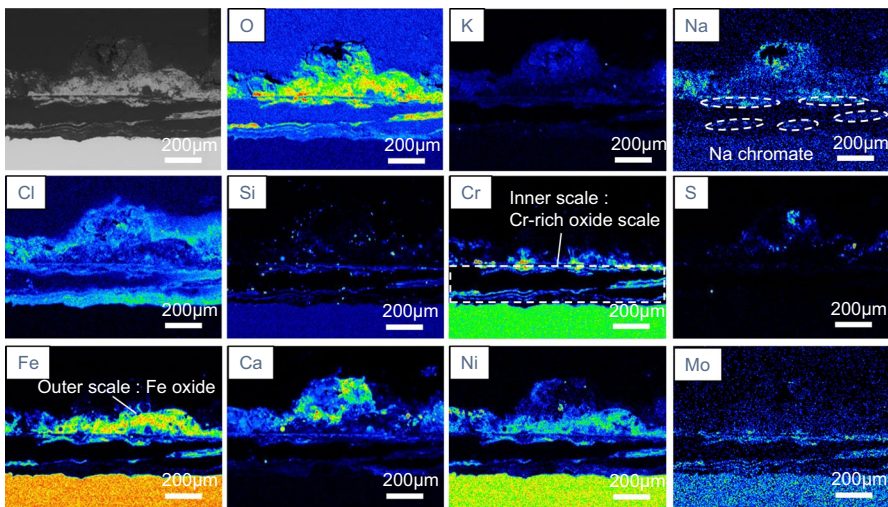


Fig. 8 Elemental distribution maps of the cross section of QSX5 embedded in the tube side ash after corrosion

Figure 7 shows an electron probe micro-analyzer (EPMA) map of each element in the oxide scale that formed on the SUS310S specimen after the temperature gradient corrosion test for 100 h. Although chlorine was detected over a wide area in the oxide scale, this might be due to contamination from the remaining ash and which occurred during polishing by oil. The regions where a strong chlorine signal was detected mainly corresponded to the ash, thus it was difficult to

confirm chloride formation in the corrosion product based on this EPMA analysis. The outer porous oxide scale mainly consisted of an Fe-rich oxide and Cr is also detected in the Fe-rich oxide scale. The inner scale with a layer-by-layer structure mainly consisted of Cr-rich oxide but Ni + Fe oxides were also detected. Ca, K and Na were found not only in the ash but also in the areas of Cr oxide in the outer and inner oxide scale, suggesting that alkaline chromates had formed. Figure 8 shows the EPMA maps of each element in the oxide scale formed on the QSX5 specimen after the temperature gradient corrosion test for 100 h. The outer porous oxide scale consisted of mainly Fe-rich oxide, which contains a relatively high Ni content. Cr oxide was also observed locally below the outer Fe-rich oxide scale. Ca and Na were also detected in the inner Cr-rich oxide scale. K was mainly detected in the ash area. The inner scale with a layered structure mainly consisted of Cr-rich oxide, but Fe, Ni, Mo, and Si were also detected. Indistinct chlorine distribution in the oxide scale in Fig. 8 could be also due to contamination during specimen preparation as mentioned above.

Characterization of Corrosion Products by XRD

Figure 9 shows X-ray diffraction patterns of the SUS310S and QSX5 specimens after the temperature gradient corrosion test for 100 h. In the case of the SUS310S, γ -Fe from the substrate, Fe_2O_3 , and Cr_2O_3 were identified from the main scale component, and Na, and Ca chromates, which were confirmed by EPMA, were also identified but K chromate was not detected. γ -Fe, Fe_2O_3 , Cr_2O_3 , Ca chromate, and the ash components NaCl, and KCl were also identified in the QSX5 specimen; however, Na and K chromates were not found even though they were detected by EPMA. It is possible that the amounts of those corrosion products formed on the QSX5 specimen were too small to be detected by conventional XRD.

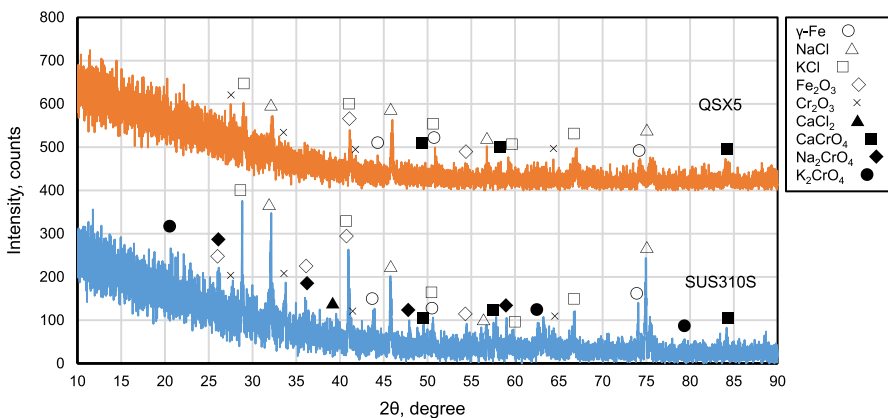


Fig. 9 X-ray diffraction profiles of SUS310S and QSX5 after 100 h of temperature gradient corrosion

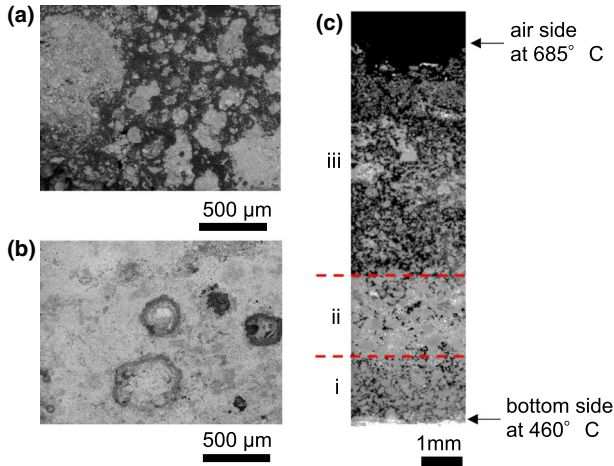
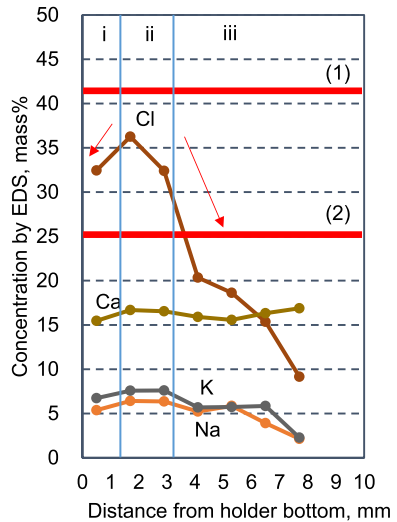


Fig. 10 Ash cross sections: **a** non-heating, **b** after heating with lid at 685 °C in air **c** after temperature gradient corrosion test

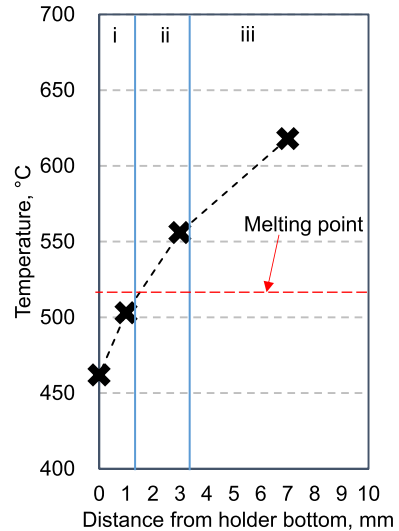
Fig. 11 Cross-sectional concentration distribution of ash by EDS after temperature gradient corrosion test. (1) Cl concentration at 685 °C with lid for 2 h, (2) Cl concentration on non-heating



Cross-Sectional Observation and Analysis of Ash

Figure 10 shows cross sections of the ash. The first (a) shows a non-heated cross section, the second (b) after being heated in a crucible with a lid at 685 °C for 2 h, and the third (c) after the temperature gradient corrosion test for 100 h. The ash before heating consisted of different sized particles and components with bright contrast were dispersed in the particles. After heating at 685 °C for 2 h, the ash became dense due to partial melting. As shown in Fig. 11, the Cl concentration in the heated ash was increased to about 41%, which is higher than that of that non-heated ash,

Fig. 12 Temperature distribution of the ash during temperature gradient corrosion test



25.5%, which might be due to densification of the ash. The ash cross section after the temperature gradient corrosion test showed a three-layered structure in the depth direction. In region 1 on the specimen side (bottom), the ash contrast was bright and porous, but the ash became dense in region 2, which was similar to heated ash at 685 °C for 2 h, and bright contrast precipitates were present. The ash in the region 3 (atmospheric side) was porous and similar to that of non-heated ash. Figures 11 and 12 show the concentration distributions of Ca, Na, K, and Cl and the temperature distribution of the ash in the depth direction after the temperature gradient corrosion test. The concentration of K, Na, and Cl is highest in region 2. The Cl concentration in regions 2 and 1 was higher than that of non-heated ash. However, the concentrations of Na, K, and Cl in region 3 gradually decreased toward the ash surface. Because the concentration of Ca was almost constant across the ash deposition, most of the alkali salts diffused from the melted region 2 as a vapor in both the surface and bottom directions. The vapor of salts diffused to the ash surface should be lost to the atmosphere during a corrosion test. However, the vapor of alkali salts diffused inwardly to the bottom side, the temperature of which is lower than the melting point, and this might contribute to the acceleration of the steel corrosion rate.

Discussion

Breakdown of the Protective Cr_2O_3 Scale

The corrosion mass change of both steels as a result of the temperature gradient corrosion test was much larger than that by the isothermal corrosion test. Both steels formed a very thin oxide scale after the isothermal corrosion test. However, the steel surface was covered by a thick and porous duplex oxide scale when the

steels were exposed to the ash with a temperature gradient. Since the temperature of the specimens was kept at 460 °C, which is lower than the melting point of the ash in both corrosion tests, steels were corroded by corrosive gas species with the same oxygen, chlorine, and salt potentials. Therefore, the temperature gradient in the ash in which the specimen was embedded has a potent effect on accelerating corrosion. The thick corrosion products formed after the temperature gradient corrosion test consisted of an outer scale of Fe-rich oxide incorporating ash components and an inner scale of Cr-rich oxide which was a layer-by-layer structure. It has been reported that SUS310S and QSX5 steels form a protective Cr_2O_3 scale in air and O_2 [15]. In the present study, a thin protective Cr-rich oxide scale was also confirmed to form locally after 100 h of corrosion when the steels were exposed in an isothermal corrosion test. Although a short-term oxidation test was not conducted in this study, it is reasonable to assume that a protective Cr-rich oxide scale was formed on both steels during the initial stage of corrosion. Then the initial protective corrosion behavior transitioned to a less protective corrosion behavior once the protective Cr-rich oxide scale was converted to corrosion products that were less protective. This transition behavior can be observed from the surface appearance shown in Figs. 3(a) and (b) that the interference-colored area with thin oxide scale regions changed to a bright-brown colored region. It is assumed therefore that the temperature gradient in ash shifts this transition time to a shorter corrosion time.

Figure 13 shows phase stability diagrams of Fe–Cl–O, Cr–Cl–O, and Ni–Cl–O at 460 °C. Fe, Cr, and Ni in Fig. 13 were calculated from the activity of those elements in the Fe–25Cr–20Ni alloy using FactSage software. The chloride region in the figures includes a gas phase having a vapor pressure of 10^{-4} atm or more. The equilibrium chlorine potential when the combustion ash was held at 460 °C in the air is given by Formula (1) from the calculation using the FactSage software.

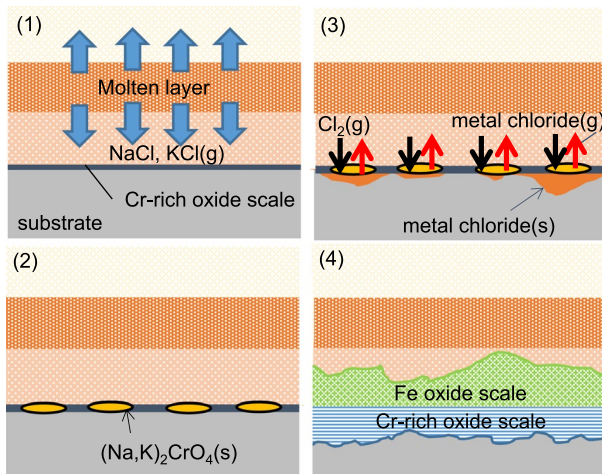
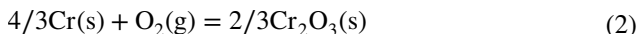


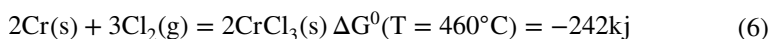
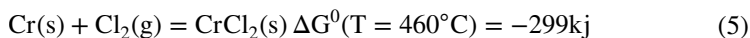
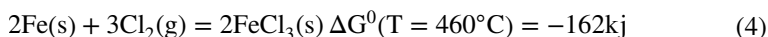
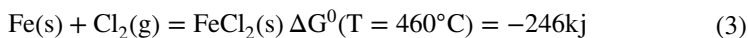
Fig. 13 Quasi-stability diagram for the Fe-25Cr-20Ni system at 460 °C with $a_{\text{Fe}}=0.62$, $a_{\text{Cr}}=0.28$, $a_{\text{Ni}}=0.11$, $P_{\text{O}_2}=0.2$ atm

$$P_{\text{Cl}_2}(T = 460^\circ\text{C}) = 8.1 \times 10^{-9} \text{ atm} \quad (1)$$

On the assumption that a Cr_2O_3 scale was formed initially, the oxygen potential at the scale/metal interface decreases to $P_{\text{O}_2} = 10^{-44}$ atm according to Formula (2) with the Cr activity, $a_{\text{Cr}} = 0.28$.

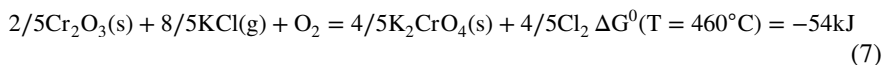


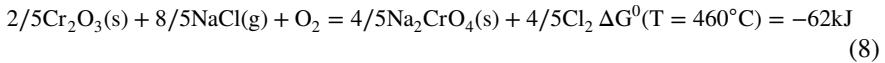
The free-energy changes in chloride formation for each element given in Formulas (3)–(6) calculated with the chlorine potential in Formula (1) and the activities of the elements in the alloy under the assumption that the chlorine potential across the Cr_2O_3 scale does not change significantly [15]. All metal components can be chloridized under a low oxygen potential below the Cr_2O_3 oxide scale.



The formation of chlorides at the scale/steel interface can cause the protective Cr_2O_3 scale to peel off due to loss of contact between scale and alloy, so one of the main factors that reduces the protectiveness of the Cr_2O_3 scale is scale exfoliation. In fact, some exfoliation was observed on a thin oxide scale formed on the specimen surface after the isothermal corrosion test as shown in Fig. 5. However, visible internal chlorination was not observed in either type of steel. Because no Cr depleted region was observed in the subsurface region of steels from the EPMA mapping, even if such scale exfoliation occurs, Cr-rich oxide scale can reform in the region where the exfoliation occurs. In addition, with this model there is no clear explanation that the temperature gradient in the ash accelerated the spallation of the protective oxide scale. Thus, scale exfoliation/spallation due to the formation of chlorides cannot be the main reason for accelerated corrosion under the temperature gradient test.

From the EPMA analysis results in Figs. 7, 8 and XRD in Fig. 9, the formation of chromates was confirmed. The vapor pressures of NaCl and KCl in the combustion ash at 460°C were calculated using FactSage as $P_{\text{NaCl}} = 3.53 \times 10^{-9}$ atm and $P_{\text{KCl}} = 1.05 \times 10^{-8}$ atm, respectively. Then, the free-energy changes of K_2CrO_4 or Na_2CrO_4 formation by formulas (7) and (8) were calculated with chlorine and oxygen potential in the atmosphere, $P_{\text{Cl}_2}(T = 460^\circ\text{C}, \text{ in the atmosphere}) = 8.1 \times 10^{-9}$ atm and $P_{\text{O}_2} = 0.2$ atm as $\Delta G_{\text{K}_2\text{CrO}_4} = -18$ kJ, and $\Delta G_{\text{Na}_2\text{CrO}_4} = -26$ kJ, respectively.



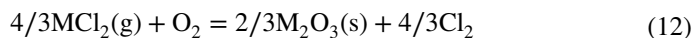


Once alkali chromates were formed, the Cr_2O_3 scale loses its protectiveness. Even if sufficient Cr remains in the alloy and a Cr_2O_3 scale is reformed below the chromate scale, a reformed Cr_2O_3 scale might react with salt vapors to form chromates again. Thus, formation of chromates could be the main reason for the long-term corrosion resistance of steels being reduced in salt vapor-containing atmospheres. Izzuddin et al. proposed a similar model for the corrosion behavior of Ni–Cr alloys in alkaline salt vapor environments [14]. When the reactions of Formulas (7) and (8) proceeded, the chlorine potential near the chromate surface is increased. The equilibrium chlorine potentials for the reactions of Formulas (7) and (8) are given by Formulas (9) and (10), respectively. The chlorine potentials are higher than that in the atmosphere (Formula (1)), which might accelerate the chlorination of steels below the less protective chromate scale.

$$P_{\text{Cl}_2} \text{eqK}_2\text{CrO}_4 = 2.0 \times 10^{-6} \text{ atm} \quad (9)$$

$$P_{\text{Cl}_2} \text{eqNa}_2\text{CrO}_4 = 3.4 \times 10^{-7} \text{ atm} \quad (10)$$

Once metal chlorides were formed, they volatilized below the chromate scale due to the high vapor pressure according to Formula (11), and the volatilized metal chlorides were then oxidized to form a porous outer oxide scale in a region of sufficient oxygen potential according to Formula (12) and released chlorine.



This chlorination-oxidation cycle, which is referred to as active oxidation, causes rapid consumption of the steel matrix without the need to supply chlorine from the atmosphere [5–7].

Effect of Temperature Gradient Across the Ash

Formation of a molten layer with a high concentration of the alkali salt in the area where the temperature was higher than the melting point of the ash was confirmed from the cross section of the ash after the corrosion test. The higher concentration of chloride/salts closer to the specimen surface than the original ash component was also confirmed, which suggests that the alkali salt vapor diffused to the low temperature region toward the specimen surface from the molten layer. Different potentials of salt vapor near the specimen surface and a molten layer could be the driving force for salt vapor flux to the surface of the specimen. Thus, it is apparent that the temperature gradient in the ash acted as the driving force to increase the flux of the alkali salt vapor from the molten layer to the specimen surface. The increase in the flux of alkali salt vapor under the temperature gradient corrosion condition could

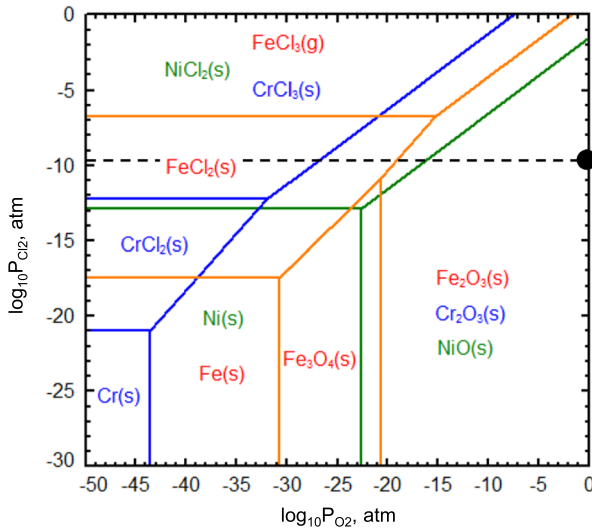


Fig. 14 Schematic of corrosion model in the combustion ash containing alkali salt in the air

accelerate the rate to extend the area of chromate scale, i.e., the rate of breakdown of the protective Cr_2O_3 scale. The protective Cr_2O_3 scale rapidly changed to a chromate scale, resulting in a shorter transition time to the less protective corrosion stage with a rapid rate of steel consumption.

Figure 14 is a schematic representation of the corrosion behavior of heat-resistant steels in a temperature gradient corrosion test. At the initial corrosion stage, a protective Cr-rich oxide scale is formed on the surface of the specimen, and the melts is formed in the temperature range above the melting point of the ash. The alkali salt vapor diffuses from the molten layer to the surface of the specimen as shown in Fig. 14 (1). Alkali salt vapors react with the Cr-rich scale to form Na and K chromates (the breakdown of the protective Cr-rich scale, Fig. 14 (2)). The chlorine partial pressure increases due to the chromate formation reaction, and more metal chloride is formed and volatilized at the scale/metal interface (Fig. 14 (3)). Once the breakdown areas cover the entire surface of the specimen within a short time, the entire surface becomes covered by a porous Fe oxide and the layer-by-layered inner layer is formed (Fig. 14 (4)). Deposit-induced corrosion as this study is described as occurring in two stages: an “incubation stage” in which corrosion is slow and then a “propagation stage” in which corrosion is rapid [17]. Therefore, it is presumed that the corrosion rate of heat-resistant steel changes rapidly due to the breakdown of the Cr_2O_3 scale.

In this experiment, QSX5 demonstrated higher corrosion resistance than SUS310S. The content of Mo and Si is higher in QSX5. The formation and maintenance of the protective Cr_2O_3 scale is known to be improved by the addition of Si due to formation of a SiO_2 layer below the Cr_2O_3 scale [18]. The addition of Mo to Ni–Cr alloys was also reported to promote a Cr_2O_3 scale and reduce the rate of high-temperature oxidation [19]. Therefore, it is presumed that the higher corrosion

resistance of QSX5 compared to SUS310S can be attributed to the effects of adding Si and/or Mo, but further detailed studies are needed to clarify the effects of these elements.

Conclusions

The effect of the temperature gradient in the ash on the corrosion resistance of super-heater tube material was investigated. The obtained results can be summarized as follows:

- (1) The corrosion mass loss after temperature gradient corrosion at a high atmospheric temperature was greater than that after isothermal corrosion, even where the temperature of the specimen was the same. In both corrosion tests, QSX5 showed higher corrosion resistance than SUS310S.
- (2) The corrosion behavior can be explained as a chlorination induced accelerated oxidation after the breakdown of the protective Cr-rich oxide scale. The Cr-rich oxide scale lost its protective ability due to the formation of alkali chromates caused by a reaction between the protective Cr-rich scale and the alkali salt vapor.
- (3) The effect of the temperature gradient in the ash is to accelerate the breakdown of the Cr-rich scale by increasing the flux of the alkali salt vapor from the molten layer to the specimen surface.

Acknowledgments A part of this work was conducted at the Hokkaido University, supported by “Nanotechnology Platform Program” of the Ministry of Education, Culture, Sports, Science and Technology (MEXT), Japan, Grant Number JPMXP09A21HK0064.

Author Contribution TF, HT, SH contributed to conception and design of study. TF contributed to acquisition of data. TF, SH contributed to analysis and/or interpretation of data. TF contributed to drafting the manuscript. TF, SH contributed to revising the manuscript critically for important intellectual content. HT, SH contributed to approval of the version of the manuscript to be publish.

Funding No funding was received for conducting this study.

Declarations

Conflict of interest The authors declare that they have no conflict of interest.

References

1. Q. Zuopeng, R. Zhong, L. Wang, W. Zhao, X. Tian, and H. Wang, *Journal of Physics: Conference Series* **1649**, 012031 (2020).
2. J. Singh, H. Vasudev, S. Singh, *Materials Today: Proceedings* (2020).
3. W. Wang and Z. Liu, *Journal of Physics: Conference Series* **1635**, 012087 (2020).
4. Kawahara, *Corrosion Science* **44**, 223–245 (2002).
5. S.-H.Nickolas J. Themells, M. J. Castaldi, *Journal of Thermal Spray Technology* **16**(1) (2007).

6. J. M. Oh, M. J. McNallan, G. Y. Lai, M. F. Rothman, *Metallurgical Transactions A*, **17A**, 1087–1094 (1986).
7. Q. Zuopeng, R. Zhong, L. Wang, W. Zhao, X. Tian, and H. Wang, *Earth and Environmental Science* **598**, 012008 (2020).
8. J. Phother-Simon*, T. Jonsson, J. Liske, *Corrosion Science* **167**, 108511 (2020).
9. S. Karlsson, J. Pettersson, L.-G. Johansson, and J.-E. Svensson, *Oxid Met* **78**, 83–102 (2012).
10. J. Pettersson, N. Folkesson, L.-G. Johansson, and J.-E. Svensson, *Oxid Met* **76**, 93–109 (2011).
11. Kent O. Davidsson, L.-E. Åmand, B. Leckner, *Energy and Fuels* **21**, 71–81 (2007).
12. S. Karlsson, L.-E. Åmand, and J. Liske, *Fuel* **139**, 482–493 (2015).
13. J. Eklund, A. Persdotter, I. Hanif, S. Bigdeli, and T. Jonsson, *Corrosion Science* **189**, 109584 (2021).
14. H. Izzuddin, S. Hayashi, S. Yoneda, T. Kogin, E. Ishikawa, M. Noguchi, *Materials and Corrosion*, 1–12 (2020)
15. D. J. Young, *High Temperature oxidation and corrosion of Metals* (2016).
16. B. S. Covino, Jr., J. H. Russell, S. D. Cramer, et al., *Conference: Corrosion 2003*, Paper No. 3718
17. N. Birks, G. H. Meier, and F. S. Pettit, *Introduction to High Temperature Oxidation of Metals*, 2nd ed (Cambridge University Press, Cambridge, 2006).
18. H. E. Evans, D. A. Hilton, R. A. Holm, and S. J. Webster, *Oxidation of metals*, **19**(1/2) (1983).
19. S.-J. Park, S.-M. Seo, Y.-S. Yoo, H.-W. Jeong, and H. J. Jang, *Materials* **12**, 2934 (2019).

Publisher's Note Springer Nature remains neutral with regard to jurisdictional claims in published maps and institutional affiliations.

Springer Nature or its licensor holds exclusive rights to this article under a publishing agreement with the author(s) or other rightsholder(s); author self-archiving of the accepted manuscript version of this article is solely governed by the terms of such publishing agreement and applicable law.

Authors and Affiliations

T. Furugaki¹ · H. Takahashi¹ · S. Hayashi²

H. Takahashi
hiromitu@takuma.co.jp

S. Hayashi
hayashi@eng.hokudai.ac.jp

¹ Takuma Co., LTD, 2-2-33, Kinrakuji-cho, Amagasaki, Hyogo 660-0806, Japan

² Faculty of Engineering, Division of Materials Science and Engineering, Hokkaido University, Kita13 Nishi8, Sapporo 060-8628, Japan